Electronic Supplementary Material (ESI) for Journal of Materials Chemistry B.

Pt(II) metallacycles encapsulated by Ferritin enable precise cancer combination chemo-photodynamic therapy

Xuehong Min,[‡a] Ming Li,[‡c] Wenjing Zhang,[‡c] Run-Hao Li,[b] Zhe Zhang,[d] Pingshan Wang,[d] Weide Su,[c] Feng Li,*[c] Yue Sun,*[b] Yi Liu,*[b]

[a] Wuhan Business University, Wuhan 430056, P. R. China.

[b] Key State Key Laboratory of Separation Membrane and Membrane Process & Tianjin Key Laboratory of Green Chemical Technology and Process Engineering, School of Chemistry, Tiangong University, Tianjin 300387, P. R. China.

[c] State Key Laboratory of Virology, Wuhan Institute of Virology, Center for Biosafety Mega-Science, Chinese Academy of Sciences (CAS), Wuhan 430071, P. R. China.

[d] Institute of Environmental Research at Greater Bay Area, Key Laboratory for Water Quality and Conservation of the Pearl River Delta, Ministry of Education, Guangzhou University, Guangzhou 510006, P. R. China.

‡ These authors contributed equally to this work.

1 Experimental Section

1.1 Synthesis of precursor 3

Precursor **3** was synthesized following a reported procedure.[1] the residue was purified by column chromatography on silica gel. Product: red solid. ^{1}H NMR (400 MHz, Acetone-d_6): δ 8.91 (d, J = 1.9 Hz, 2H), 8.60-8.55 (d, J = 6.2 Hz, 2H), 8.10-8.03 (m, 3H), 7.95 (d, J = 9.0 Hz, 2H), 7.8-7.80 (d, J = 8.6 Hz, 4H), 7.48-7.46 (m, 2H), 7.44 - 7.42 (d, J = 8.6 Hz, 4H), 7.14-7.12 (d, J = 9.0 Hz, 2H). ^{13}C NMR (101 MHz, Acetone-d_6) δ 158.69 (s), 152.92 (s), 148.67 (s), 147.89 (s), 145.37 (s), 135.31 (s), 135.27 (s), 133.78 (s), 133.00 (s), 128.60 (s), 127.16 (s), 123.97 (s), 123.81 (s), 119.29 (s), 114.95 (s), 114.08 (s), 75.88 (s).

1.2 Molecular calculation of protein binding capacity

The X-ray structure of HFn monomer was downloaded from the RCSB Protein Data Bank (PDB code: 1FHA). The binding site is predicted by using the Minimize Ligands module in Discovery Studio and adopting the CDOCKER. The most tightly bound conformation was selected for further analysis, which has displayed highest -CDOCKER interaction energy of 34.9111 kcal/mol.

1.3 Transmission electron microscopy

The samples were dropped onto a carbon-coated copper grid and incubated for 3 min, followed by negative staining with 2.0% phosphotungstate (PTA) for 2 min and drying at room temperature. The grid was observed under an FEI Tecnai G2 20 TWIN electron microscope equipped with an Olympus Cantega G2 bottom-mounted CCD TEM camera. ImageJ Software (NIH, USA) is used to process the TEM images.

1.4 Measurement of hydrodynamic size and zeta potential

Two measurements of HFn-PtM were performed on a Zetasizer® Nano ZS (Malvern Instruments, Malvern, UK) at 25°C as described previously. The samples were filtered with 0.1 μm syringe filters and then centrifuged at 10000 rpm for 3 min before hydrodynamic size measurement. For zeta potential measurement, samples were in 0.25 × PBS (34.25 mmol/L Na Cl, 0.675 mmol/L KCl, 2.5 mmol/L Na_2HPO_4, 0.5 mmol/L KH_2PO_4, pH 7.2).

1.5 Cell culture

MCF-7 cells were incubated in Dulbecco's MEM (DMEM) supplemented with fetal bovine serum (10%) and penicillin/streptomycin (1%) in a humidified atmosphere incubator with 5% CO_2 at 37°C. HFF-1 cells were incubated in DMEM medium containing 15% FBS and CT26 cells were cultured in RPMI 1640 medium containing 10% FBS. Other conditions

are the same as above. The cells were isolated by trypsin when the confluence of the cells came to 60~80%.

1.6 Analysis of cellular uptake of the platinum contents by ICP-MS

MCF-7 cells were seeded into 12-well plates at a density of 2.5×10^5 cells and grew for 24 h. Then, the cells were incubated with 10 μM HFn-PtM for 5 h and 15 h, respectively. Finally, the cells were harvested, washed and collected. The Pt content in cells was analyzed by Flexar/ NexlON300X (PerkinElmer, USA).

1.7 Statistical analysis.

Statistical analysis was performed using a one-way ANOVA followed by Tukey's multiple comparison test analysis ($P < 0.05$) to denote significant differences.

2 Supporting Figures

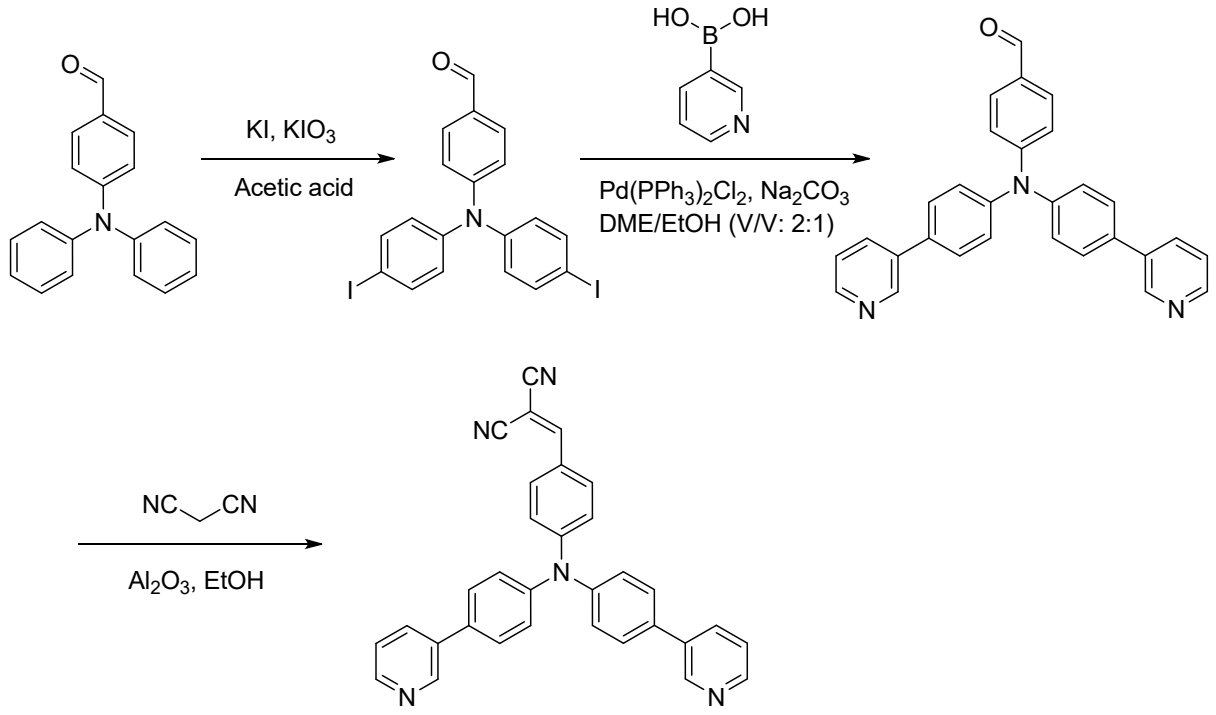

Figure S1. Preparation of precursor **3**.

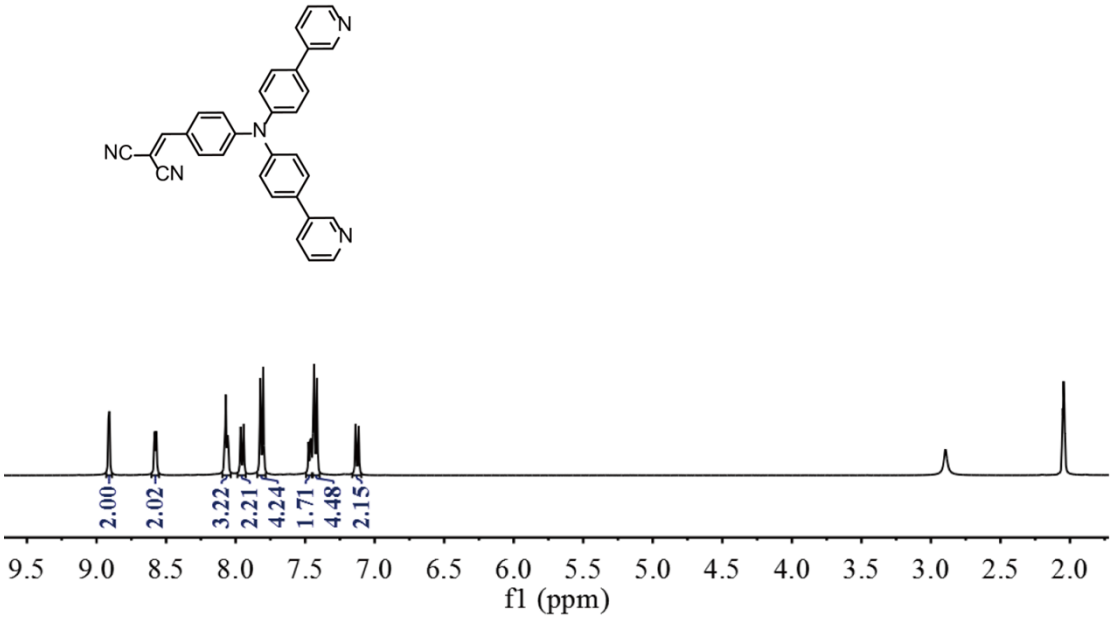

Figure S2. ^{1}H NMR spectra of precursor **3** in acetone-d_6.

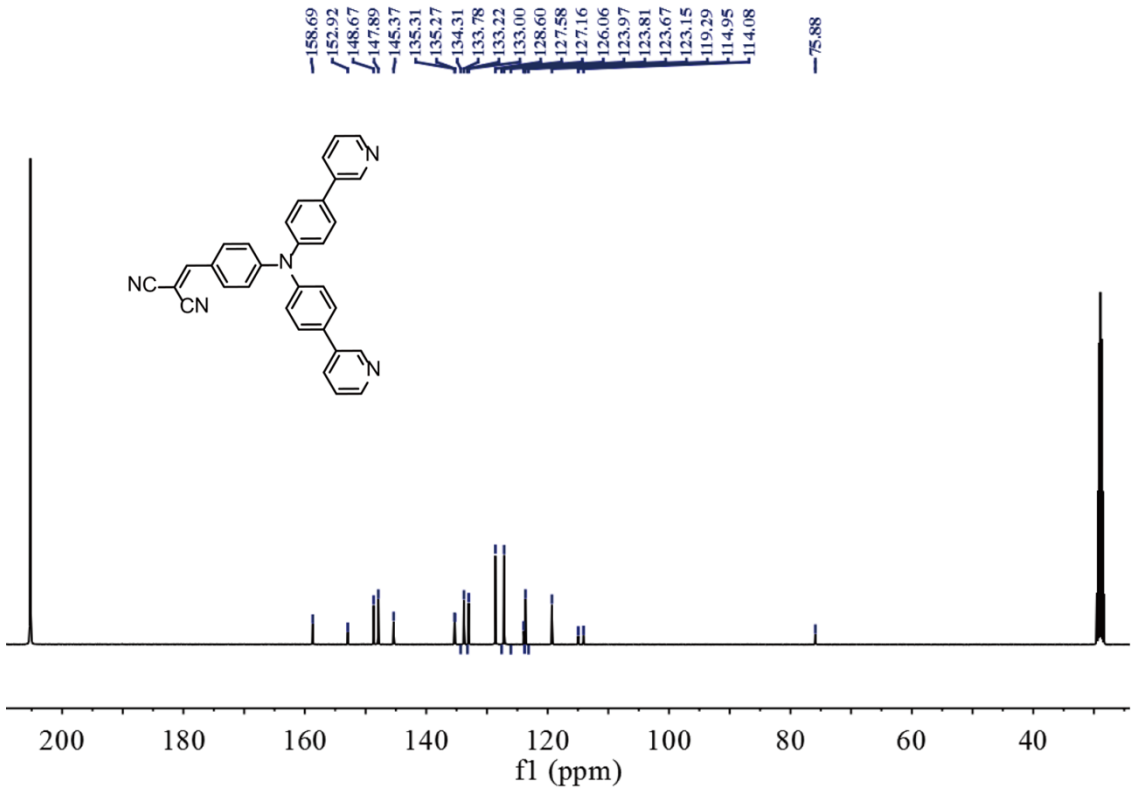

Figure S3. ^{13}C NMR spectra of precursor **3**.

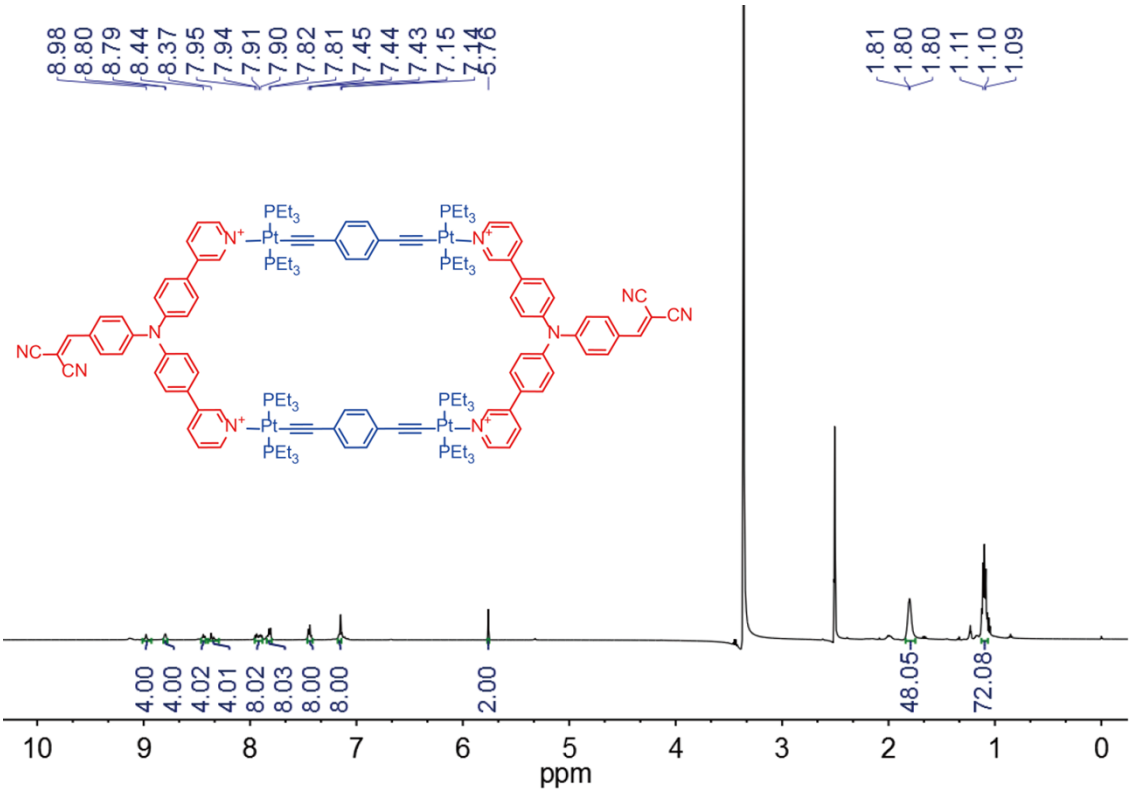

Figure S4. ^{1}H NMR spectra of metallacycle PtM in DMSO-d_6.

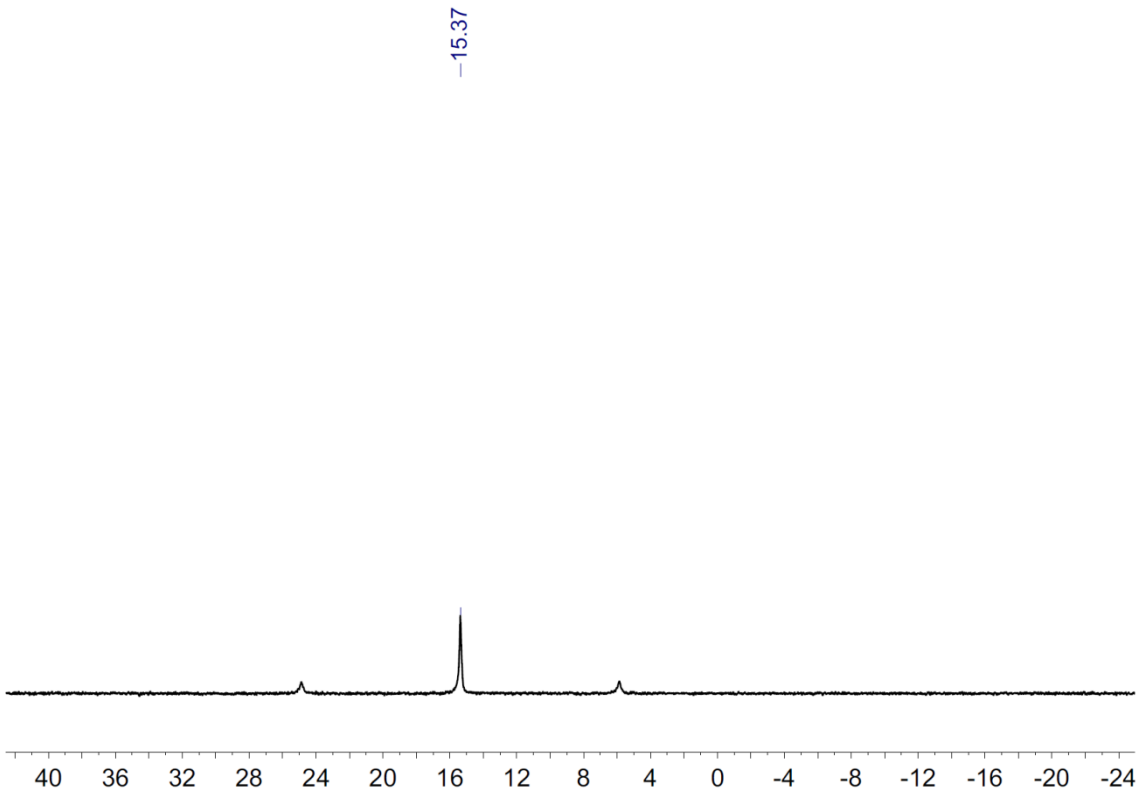

Figure S5. $^{31}P\{^{1}H\}$ NMR spectra of PtM in DMSO-d_6.

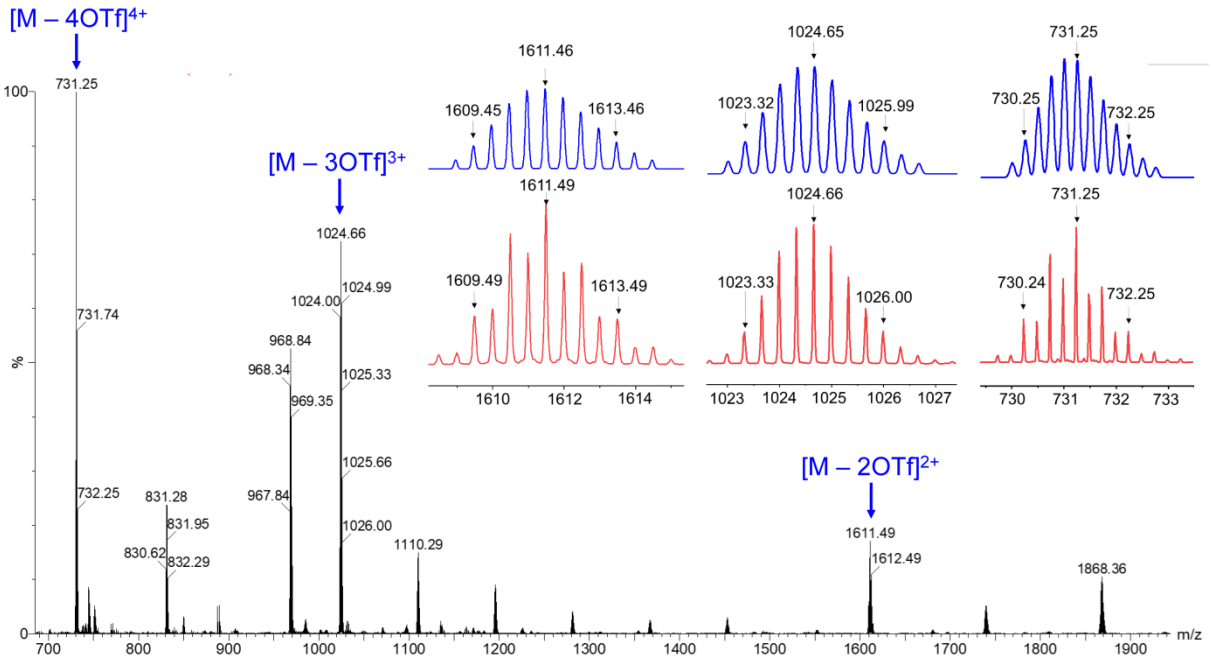

Figure S6. ESI-MS for metallacycle PtM.

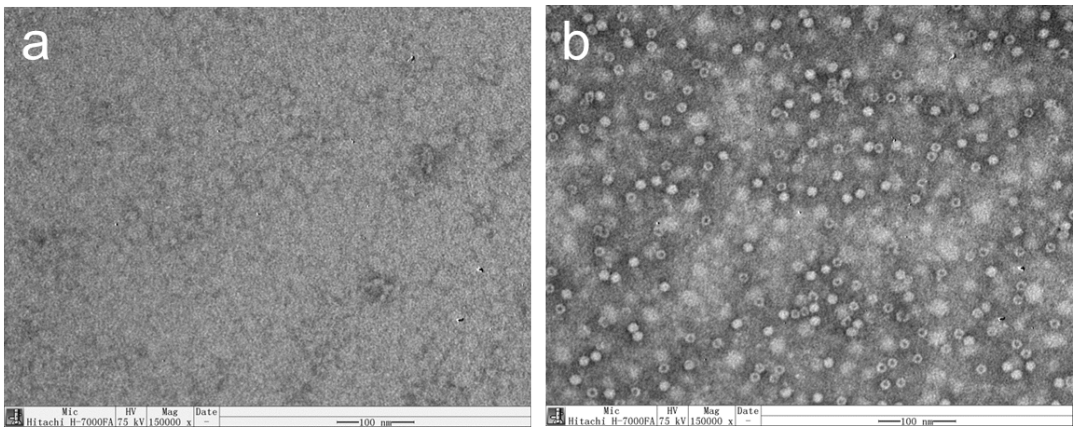

Figure S7. TEM Images of (a) Depolymerized HFn and (b)HFn-PtM after assembly.

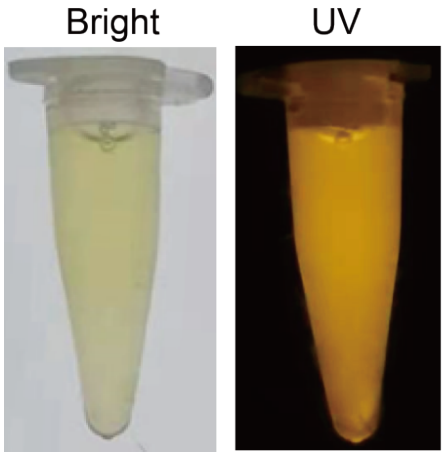

Figure S8. Images of HFn-PtM in the aqueous solution under 365 nm UV excitation.

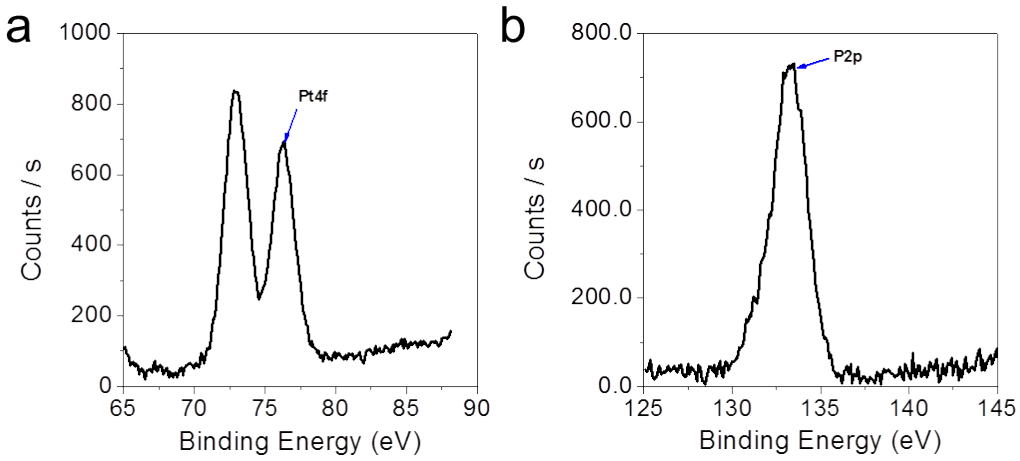

Figure S9. Component peak fitting of the XPS spectra for (a) Pt4f and (b) P2p in the HFn-PtM.

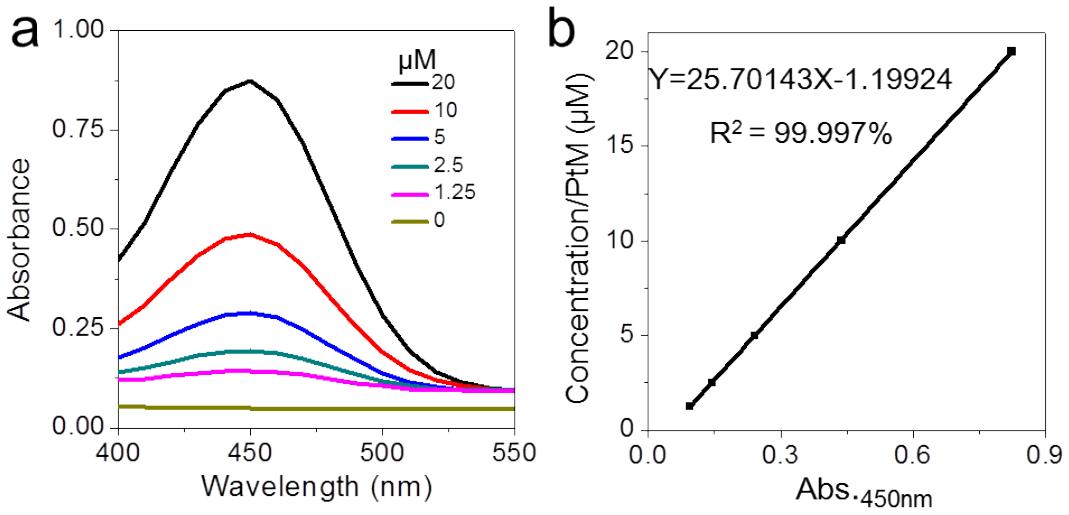

Figure S10. Correlation between absorbance and concentration of PtM molecules. (a) UV-Vis absorption spectra of PtM molecules at different concentrations in a ferritin solution. (b) A linear relationship between absorbance and concentration of PtM molecules.

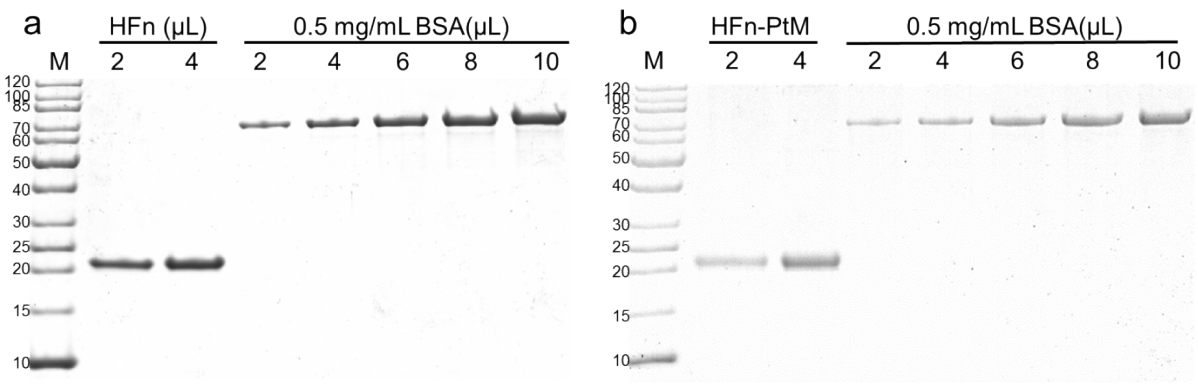

Figure S11. Protein quantification of (a) HFn and (b) HFn-PtM based on SDS-PAGE.

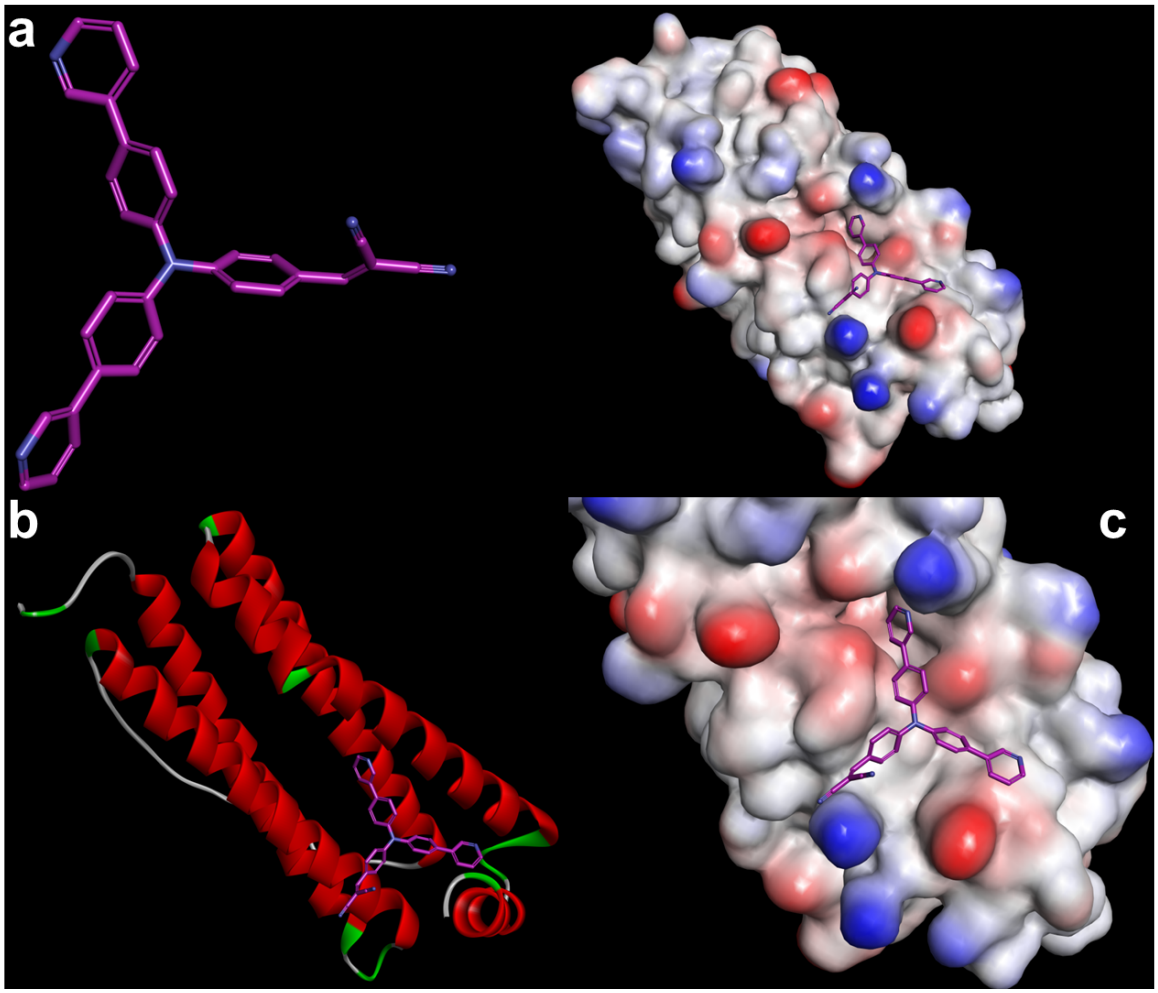

Figure S12. (a) Schematic of precursor 3 binding to HFn monomer (protein database code: 1FHA). (b) Internal binding of residues in the active pocket. (c) Enlarged view of the active pocket. (The Minimize Ligands module in Discovery Studio 2019 was used for molecular docking)

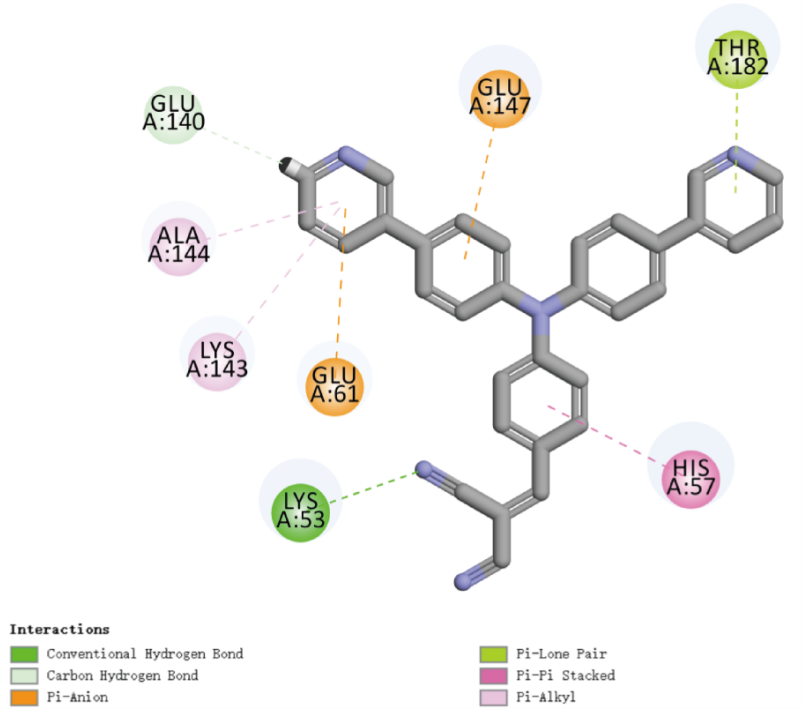

Name	Distance(Å)	Categoy	Type
LYS53	2.74	Hydrogen Bond	Conventional Hydrogen Bond
GLU140	2.54	Hydrogen Bond	Carborn Hydrogen Bond
ALA144	4.65	Hydrophobic	Pi-Alkyl
LYS143	5.18	Hydrophobic	Pi-Alkyl
HIS57	4.09	Hydrophobic	Pi-Pi Stacked
GLU61	4.29	Electrostatic	Pi-Anion
GLU147	3.78	Electrostatic	Pi-Anion

Figure S13. Analysis of the optimal conformational interaction between HFn monomers and precursor **3** in the metallacycle PtM.

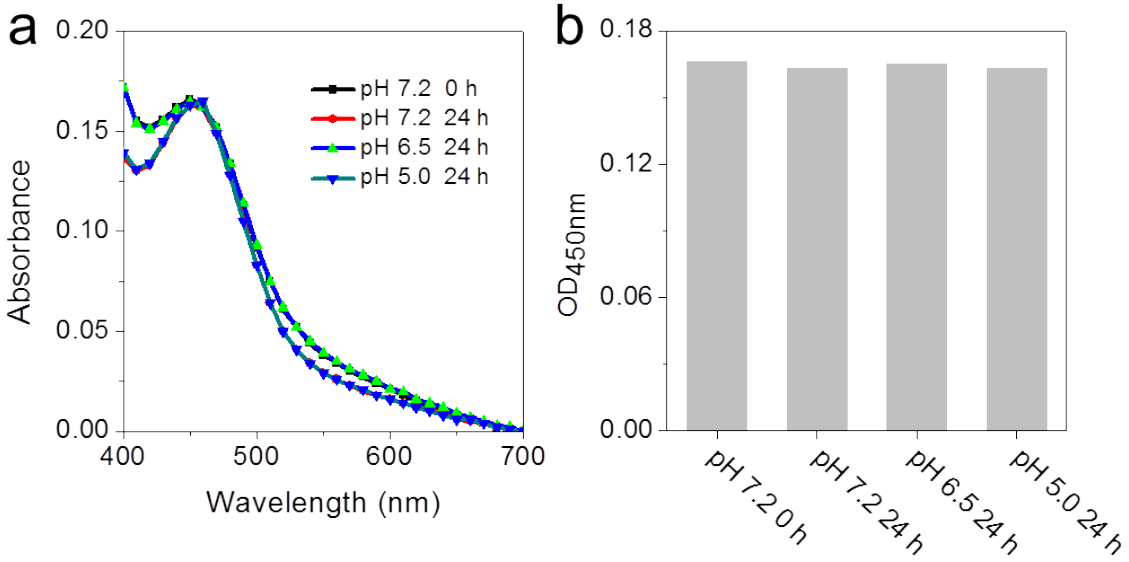

Figure S14. (a) The UV-Vis absorption spectra of HFn-PtM and (b) the absorption values at 450 nm after 24 h incubation at different pH values using dialysis bags at 37°C.

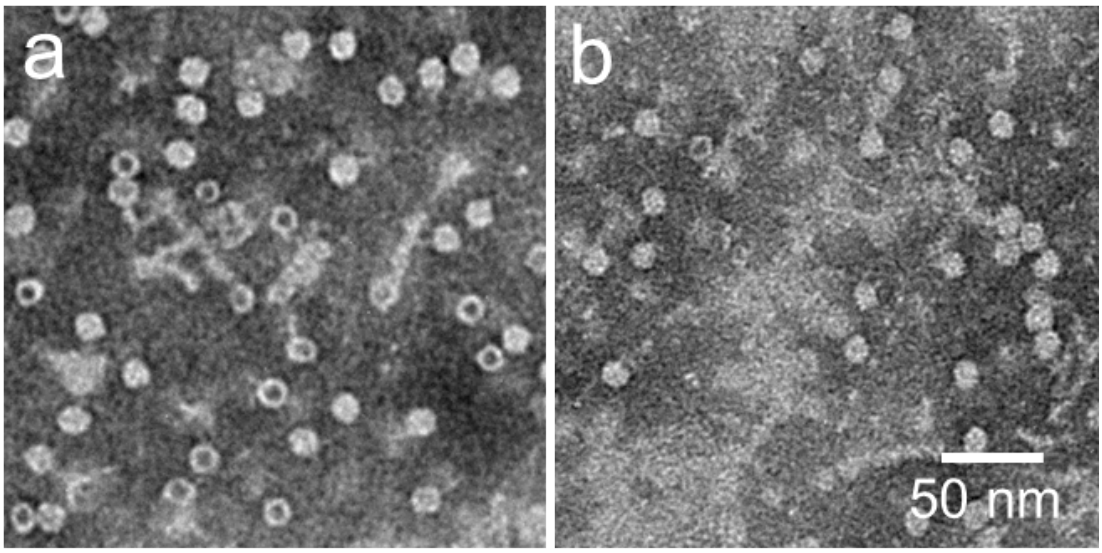

Figure S15. TEM images of HFn-PtM after 24 h incubated with PBS (a) and 10% serum (b) at 37°C respectively.

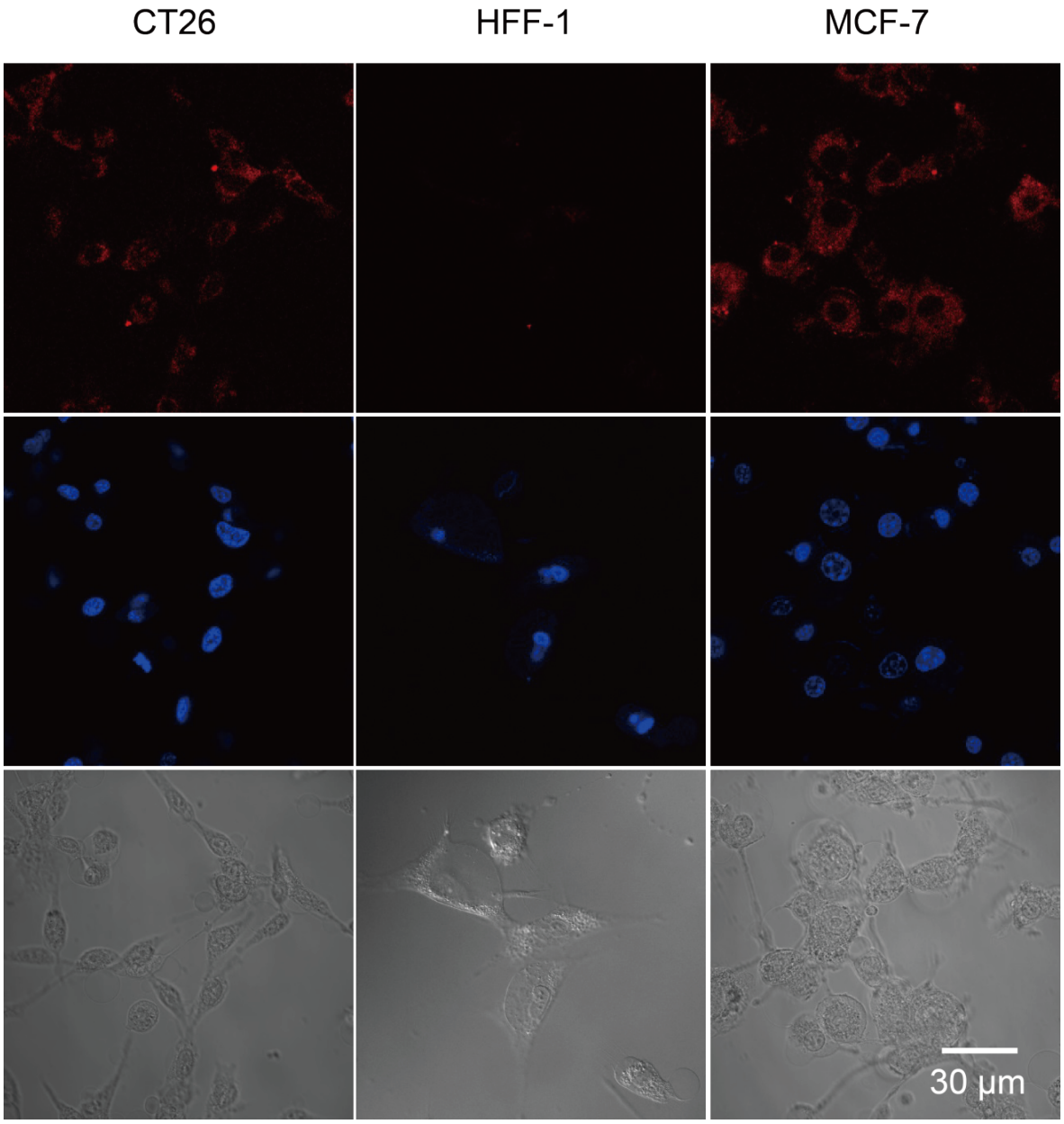

Figure S16. Confocal fluorescence images of CT26, HFF-1 and MCF-7 cells incubated for 4 h with 10 μM HFn-PtM. Nuclei were stained with Hoechst 33258 (blue).

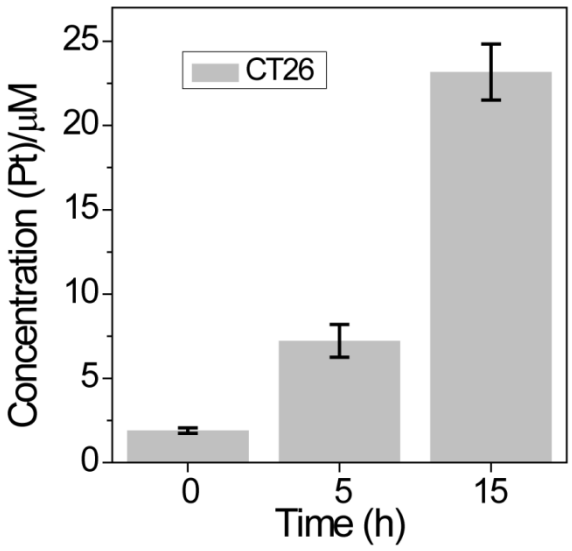

Figure S17. Platinum content of CT26 cells (2 x 10^6) after different incubation times based on ICP-MS measurements.

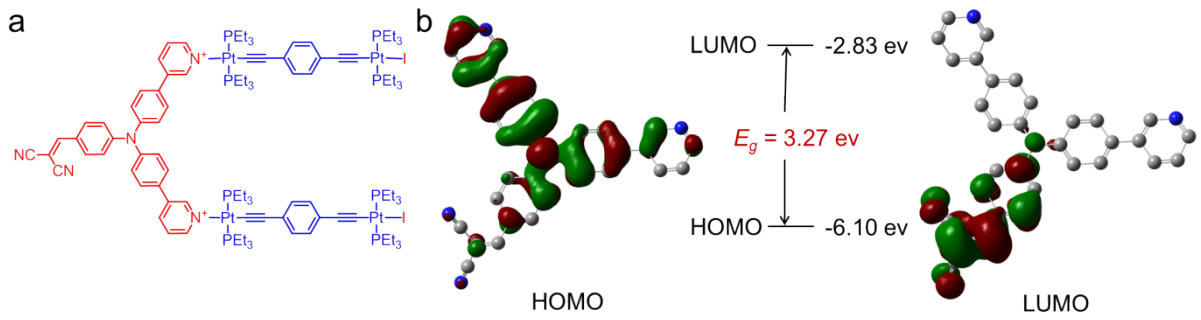

Figure S18. (a) The half complex structures of PtM. (b) Optimized structures of the HOMO and LUMO of precursor 3 at S_0 were calculated by time-dependent DFT (Gaussian 09/B3LYP/LANL2DZ).

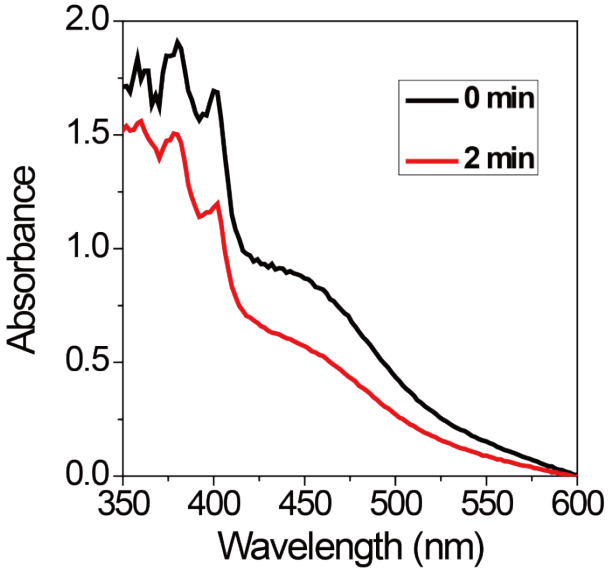

Figure S19. Absorption spectra of ABDA in the presence of HFn-PtM without irradiation and after 2 min of irradiation.

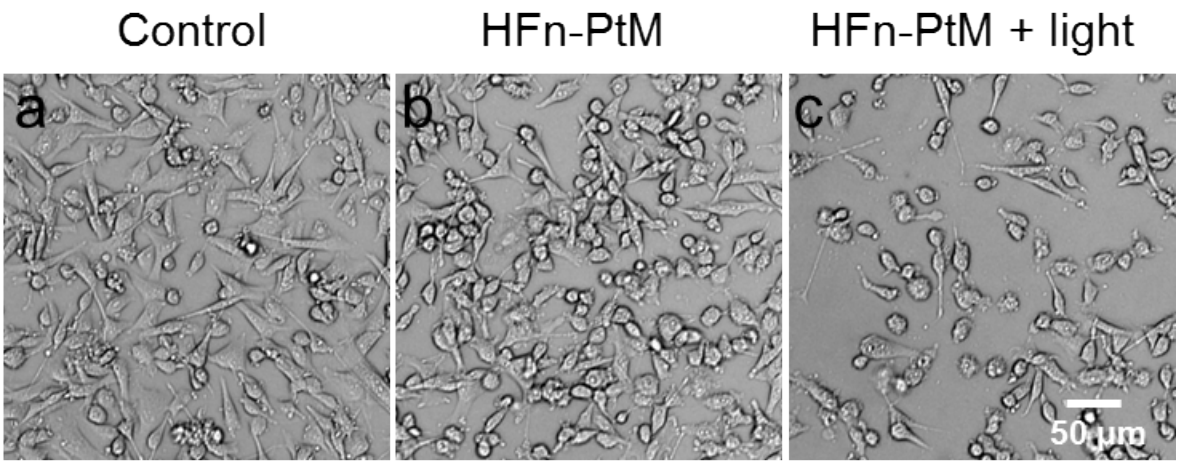

Figure S20. Inverted images of CT26 cells incubated without (a) and with10 μM HFn-PtM for 4 h, treated without (b) or with (c) white light irradiation (200 mW/cm^2, 10 min) and cultured for another 24 h.

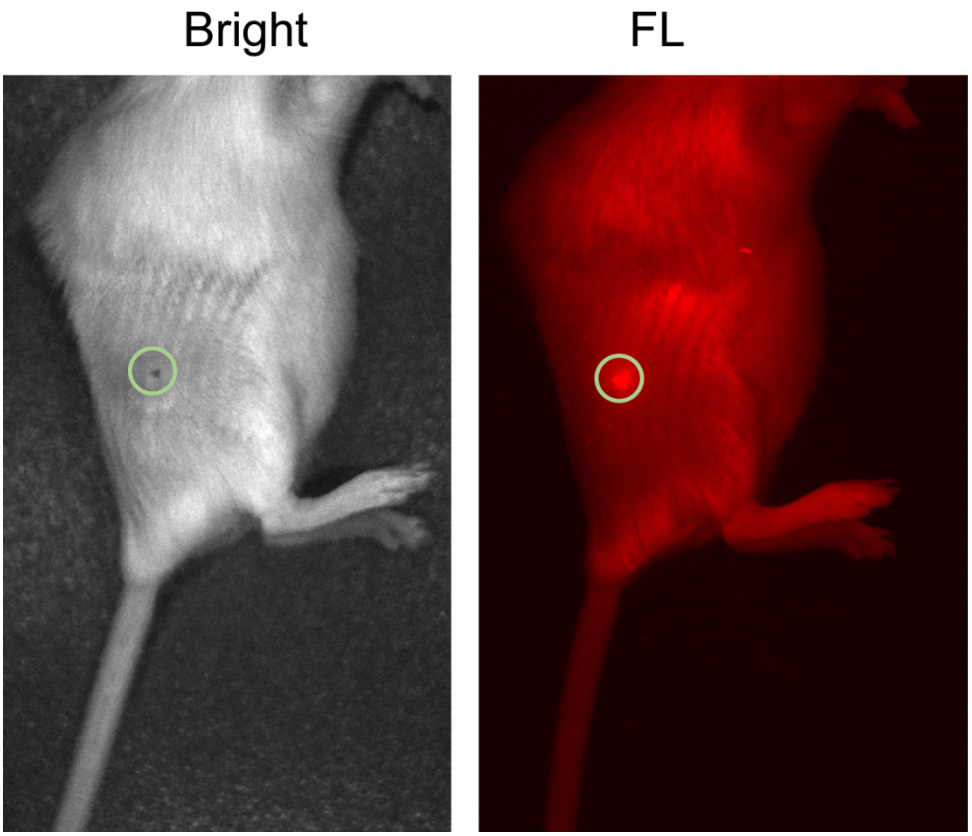

Figure S21. Fluorescence distribution image in mice 48 h after intravenously (i.v.) injection.

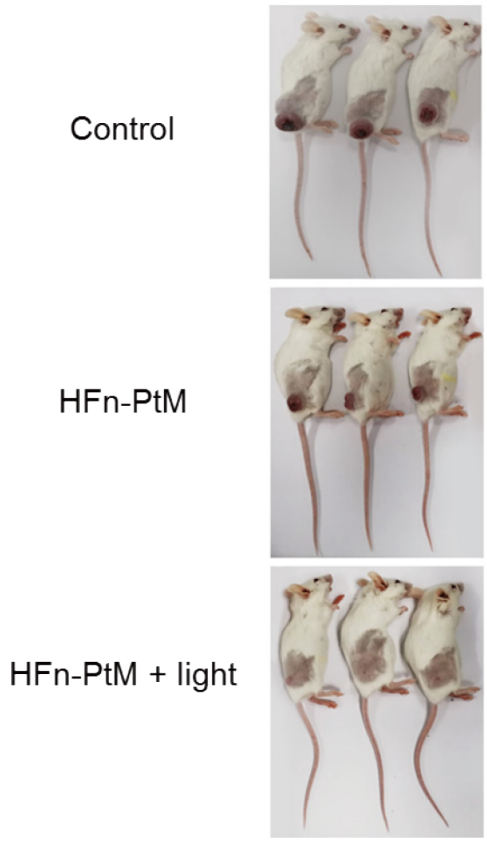

Figure S22. The bright images of mice bearing CT26 tumor post various treatments.

3. References

1. X. Liu, Y. Qin, J. Zhu, X. Zhao; T. Cheng, Y. Jiang, H. Sun and L. Xu, Acid-induced tunable white light emission based on triphenylamine derivatives, *Chin. Chem. Lett.* 2021, **32**, 1537-1540.